Journal of Glaciology

Article

†The title of this article has been amended, see Corrigendum doi.org/10.1017/jog.2022.104

Cite this article: Hong J, Talalay P, Man T, Li Y, Fan X, Li C, Zhang N (2022). Effect of high-pressure sintering on snow density evolution: experiments and results. *Journal of Glaciology* **68**(272), 1107–1115. https://doi.org/10.1017/jog.2022.11

Received: 27 August 2021
Revised: 2 February 2022
Accepted: 3 February 2022
First published online: 6 April 2022

Key words:
Compressive strength; density evolution; high pressure; polar region; sintering; snow

Author for correspondence:
Jialin Hong, E-mail: hjl2398@126.com;
Nan Zhang, E-mail: znan@jlu.edu.cn

cambridge.org/jog

Effect of high-pressure sintering on snow density evolution: experiments and results†

Jialin Hong[1,2], Pavel Talalay[1], Teng Man[3,4], Yazhou Li[1], Xiaopeng Fan[1], Chuanjin Li[5] and Nan Zhang[1]

[1]Polar Research Center, College of Construction Engineering, Jilin University, Changchun 130026, China; [2]College of Materials Science and Engineering, Jilin University, Changchun 130000, China; [3]Institute of Advanced Technology, Westlake Institute for Advanced Study, Hangzhou 310024, Zhejiang Province, China; [4]School of Engineering, Westlake University, Hangzhou, Zhejiang 310024, China and [5]State Key Laboratory of Cryospheric Science, Northwest Institute of Eco-Environment and Resources, Chinese Academy Sciences, Lanzhou, China

Abstract

Very few studies have emphasized the effects of high-pressure sintering on snow density evolution, even though snow as a type of engineering material is widely used in construction engineering in cold regions for snow pavement, snow runway and polar infrastructure. This study presents new experimental results of snow densification under high pressures of up to 100 MPa for a temperature range from −3.5 to −17.3°C and uniaxial compression at the temperature of −10°C and constant strain rates from 5×10^{-4} to 10^{-1} s^{-1}. Results reveal that density evolution of snow to ice under high-pressure sintering can be achieved in a wide temperature range within a duration as short as 5 min. The compressive strength of snow-sintered ice was ~1.2–2.2 times as large as that of water-frozen ice reported by previous work. The orthogonal experiment showed that pressure is a more significant factor affecting the final density in comparison with sintering temperature and time. The increased rates of ice fabrication, low limitations on temperature and reliable sintered snow strength indicate that snow-ice engineering, such as airport construction in Greenland and Antarctica, can be improved by high-pressure sintering of snow to overcome the harsh environment.

Introduction

Snow as a material is widely used in sculpture, shelter, igloo, foundation, winter pavement, snow runway in cold regions and is also an agent in forming the pore structure of powder shaping technologies (Ramseier, 1967; German, 2014; White and McCallum, 2018). As early as 1913 Koch and Wegener used processed snow to build bridges across crevasses on a Greenland expedition, while snow runways have been constructed for landing aircraft in polar regions since 1925 (Ramseier, 1967). Processed snow was also used as foundations for snow arches spanning a 12.5 m wide trench at Camp Century, Greenland (Tobiasson and Donald, 1966). Recently, a novel balloon method used in the East Greenland Ice-core Project (EGRIP) shed light on trench construction techniques in polar regions. The EGRIP trenches were covered with snow roofs by blowing snow back onto inflated balloons, where ~50 cm in height deformations were identified after one year of service (J.P. Steffensen, pers. comm.). Many techniques have been used to pressure sinter the snow to increase its density and strength depending on in situ natural atmospheric temperatures (Kingery, 1960). The most difficult aspect of the process is that, for required density and strength, snow is usually sintered at relatively high temperature (close to 0°C) and over timescales on the order of months (Ramseier, 1967). At low temperatures, techniques involving the addition of heat and/or water have been used with unsuccessful results due to unreliable performance of heating equipment and massive maintenance for water circulation, and are often fuel-intensive limiting their practical feasibility for large-scale use (Abele and others, 1968). A better understanding of snow density (hereinafter referred to as density) evolution during high-pressure sintering is beneficial for easy, broad and efficient utilization of snow as a promising material for construction in places such as Greenland and Antarctica or in temperate areas with a heavy annual snow accumulation where snow as a material is abundant and may be used for constructing camps, igloos, trenches and snow runways.

The process by which snow particles bond together at temperatures below the melting point through external pressure occurs by pressure sintering in the same fashion as in powder metallurgy and ceramics (Ramseier, 1966; Maeno and Ebinuma, 1983). There are numerous papers published on pressure sintering of snow. Most focus on the implications for snow densification in polar regions, addressing the temperature influence on technologies for snow runway construction (Albert, 1963; Abele and Frankenstein, 1967; Abele and others, 1968; Abele, 1990), and the physical meaning of the density–depth (or age) relationship in a changing climate (Maeno and Ebinuma, 1983; Ebinuma and Maeno, 1985; Ebinuma and Maeno, 1987; Salamatin and others, 2009; Meyer and others, 2020). The US Army Cold Regions Research and Engineering Laboratory (CRREL) reported various processing methods to enhance the

sintering rate during snow densification reaching a critical density of 550 kg m^{-3} for runway construction in Greenland and Antarctica (Albert, 1963; Ramseier, 1966, 1967; Abele and Frankenstein, 1967; Abele and others, 1968; Abele, 1990). However, the sintering rate in snow runway construction is restricted by the local temperature (from near 0 to −61.7°C (Ramseier, 1966)) and applicable pressure exerted by conventional machines (for instance, 0.8–0.9 MPa from a pneumatic roller (Russell-Head and others, 1984)). Although many efforts, including heating snow, optimizing snow grain size distribution and upgrading load of processing machine, have been used to result in high density and strength, the sintering time still requires days, weeks or even months to achieve full strength (White and McCallum, 2018). Maeno and Ebinuma (1983) and Ebinuma and Maeno (1985) constructed pressure sintering diagrams of ice and performed pressure sintering experiments of pure ice particles at pressures between 0.1 and 2 MPa, and temperatures between −25 and −9°C for application to the densification of snow at polar glaciers, concluding that the densification of ice cores at the Byrd and Mizuho Stations in Antarctica can be interpreted adequately by regarding it as a phenomenon of pressure sintering. Arzt and others (1983) applied a density-pressure map for ice to snow densification at Byrd Station in Antarctica and Site 2 in Greenland, suggesting a method to predict the density profiles in other locations. The densification of snow under its own weight is also of interest in snow metamorphism and avalanche forecast (Schleef and Löwe, 2013; Wang and Baker, 2013). Wang and Baker (2013) performed compression tests using natural snow under a constant displacement rate (average at 3.5×10^{-6} m s^{-1}) with the resulting pressure increasing from 0.7 to 9 kPa at temperature −6°C and gave emphasis to the mechanism of low-density snow deformation as a combination of fracturing and sintering. Schleef and Löwe (2013) investigated the evolution of density under an external pressure ranging from 0 to 318 Pa at constant temperature −20°C and found the snow density increases with higher external pressure and lower initial density. Snow densification under high-pressure sintering has been reported to prove the feasibility of applied glaciology using snow and ice as structural materials. Diemand and Klokov (2001) produced snow-ice bricks with initial density 420–450 kg m^{-3} under pressure up to 6.87 MPa at temperatures ranging from −5 to −15°C and concluded the high-pressure sintering was a low-energy method of producing high-strength snow for construction of pavement, walls, shelters and so forth. They found that the sintering process was completed at the time of fabrication under high pressure and the temperature had little effect on the properties of the final snow bricks (Deimand and Klokov, 2001). These results highlight both the promising potential of snow-ice engineering and the ambiguous influence of pressure and temperature on snow sintering process at pressures significantly higher than natural gravity forcing and those that have been studied to date.

Therefore, the density evolution of high-pressure sintering and compressive behavior of sintered snow is investigated in this study to obtain insights into snow applications for construction engineering such as airport construction in Greenland and Antarctica, and ice road network in cold mining regions to provide vehicle access for equipment supplies and fuel.

Experimental procedure

Freshly fallen snow was collected using separate sealed plastic bags (30 × 40 cm) during the night at a temperature of −20 ± 5°C outside the Polar Research Center, Changchun, China. The snow was in a dry particle condition and no melting occurred, with grain size from 0.2 to 0.6 mm. Snow samples were stored by bags piled in a freezer at −20 ± 3°C. Pressure sintering tests were carried out with this sample settling 3 months; the original snow volume had decreased by nearly 50%. Since the focus of this study is the density evolution in intermediate and final stages of high-pressure sintering (i.e. 60% < ρ_r < 100%), two bags of snow samples were chosen from the bottom of the snow bags pile for our tests with initial density ~500 kg m^{-3}.

The low-temperature creep machine (Fig. 1a) for pressure sintering consisted of a low-temperature chamber equipped with two temperature sensors, a fixed loading steel disk connected with a load sensor, a moveable loading steel disk connected with a servo motor powered liquid hydraulic loading system, and a control system to set up sintering parameters (loading rate, pressure, pressure holding period and temperature) and record data. Temperature calibration was conducted prior to any experiments by placing an extra thermocouple in the steel die (with an inner diameter of 26 mm and a height of 100 mm) filled with snow. The difference between the outer thermocouple reading within the die along with the time required for the sample to reach the set temperature was then measured. This difference was within 2°C depending on the specific temperature, which was set between −5 and −20°C. Hereinafter the temperature described below refers to the actual snow temperature inside the die, which was stabilized within 15 min to the corresponding set temperature with the tolerance ±0.1°C. The ice melting point, T, was determined at different applied pressures P to avoid snow leakage during experiments. The ice pressure melting point was quantified based on its correlation with applied pressure (Paterson, 2010):

$$T = T_0 - \beta P, \tag{1}$$

where $\beta = 7.42 \times 10^{-8}$ K Pa^{-1} specifies the rate of change of the melting point with pressure, and $T_0 = 273.16$ K denotes the triple-point temperature of water (Paterson, 2010). At pressures of 10, 40, 70 and 100 MPa, the ice pressure melting points were calculated to be −0.732°C (0.997T_m), −2.958°C (0.989T_m), −5.184°C (0.981T_m) and −7.41°C (0.973T_m), respectively. Note that the pressure melting point is a limitation for snow sintering experiments at high pressures. The high-pressure sintering of snow was conducted at a temperature range from −3.5 to −17.3°C corresponding to specific applied pressures varying between 10 and 100 MPa as shown in Table 1.

The steel die was cooled in a freezer at −20 ± 3°C for 2 h before the snow was poured into the die to a height of ~80 mm. The die was then placed stationary on a loading disk in the low-temperature chamber of the creep machine (Fig. 1b) for 20 min before the snow was preloaded by lifting the moveable loading disk until a force of 0.5 kN (0.94 MPa) was achieved. This was done to minimize the discrepancy between the initial density during snow filling resulting in the range between 550 and 610 kg m^{-3}. The snow was compressed at a constant loading rate of 3.5 kN min^{-1} to reach the set pressure followed by constant pressure (Table 1). The total sintering time for each experiment was 60 min including the pressure-acceleration period and pressure-holding period, i.e. the time for compressing the sample at constant loading rate or constant pressure, respectively. The sintered sample length and mass were measured three times with a Vernier caliper and electronic balance following the completion of each sintering experiment in order to calculate the final density. The instantaneous axial displacement of the moveable loading disk, the applied pressure on the snow and the sintering time were recorded with a precision of ±5‰. The time interval between each experiment was at least 40 min. Three readings (corresponding to the three replicates) were recorded for each experimental condition. In total, 42 tests were performed for density evolution

https://doi.org/10.1017/jog.2022.11 Published online by Cambridge University Press

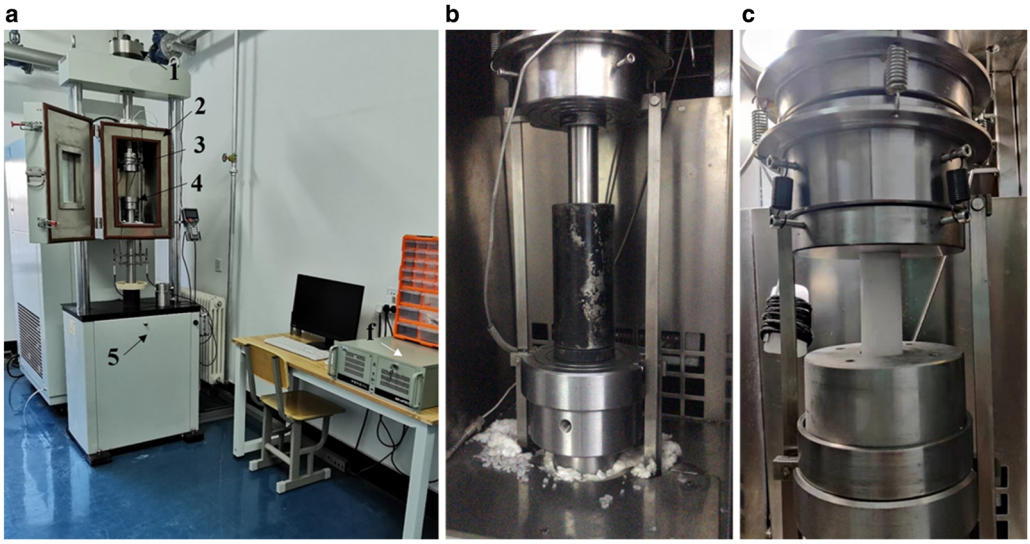

Fig. 1. (a) Low-temperature creep machine for pressure sintering test and compression test: 1 – load sensor; 2 – low-temperature chamber; 3 – fixed-loading steel disk; 4 – movable loading steel disk; 5 – servo motor (behind the cover); 6 – control system. (b) Set up for pressure sintering: steel die placed between two loading disks. (c) Set up for compression test: sintered sample sat between two loading disks with a temperature calibration sample along side.

Table 1. Pressure sintering parameters

Temperature (°C)	−3.5	−7.9	−12.5	−17.3
Homologous temperature	$0.987T_m$	$0.971T_m$	$0.954T_m$	$0.937T_m$
Applied pressure (MPa)	10	10	10	10
	40	40	40	40
	–	70	70	70
	–	80	100	100

measurements to investigate the influence of the sintering time, temperature and pressure.

The density was calculated from the recorded axial displacement based on mass conservation via the following expression:

$$\rho_x = \frac{m_f}{(1/4)\pi D^2(h_f + h_m - h_i)}, \quad (2)$$

where ρ_x is the instantaneous density (g cm^{-3}); m_f is the average snow sample mass measured by electronic balance following the completion of sintering (g); D is the diameter of the snow sample (cm); h_f is the average final height of the snow sample (cm); h_m is the maximum value of h_i (cm); and h_i is the instantaneous axial displacement of moveable lower loading disk.

We conducted unconfined uniaxial compression experiments under constant strain rates by using the same low-temperature creep machine as was used for pressure sintering tests (Fig. 1c). The chamber temperature was set to be −10.5°C, resulting in the sample temperature at −10 ± 0.2°C. The strain rate ranged from 5×10^{-4} to 10^{-1} s^{-1}. This temperature of −10°C and these strain rates are suitable for comparing our results with those of Yasui and others (2017) to investigate the strength difference between water-frozen ice and snow-sintered ice. The frost particles collected from the cooling coils of a refrigeration unit were used to sinter the sample, with grain size from 0.2 to 1 mm. Because the natural snow contains a large volume of particulate impurities, it may affect the results for comparison with that of pure ice presented by Yasui and others (2017). The compression tests under the same conditions were performed three times.

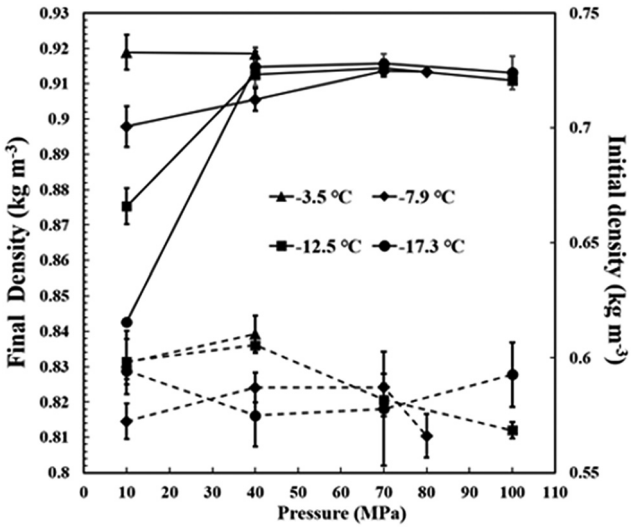

Fig. 2. Pressure dependence of final density sintered at various temperatures: solid line and dashed line represent final and initial density, respectively.

Results and discussion

Effect of pressure on final density

Figure 2 shows the effect of pressure on the final densities with an initial density ranging between 550 and 610 kg m^{-3} for samples sintered at various temperatures for 60 min. The plotted initial and final density was averaged from three replicates with std dev.. The diameter, initial and final average height of all samples are 2.6 (same as the inner diameter of the die), 7.4 and 4.8 cm, respectively. A clear enhancing effect of pressure on the final density at a lower temperature was observed. Figure 2 shows that maximum densification did not occur until the sintering pressure had increased to 40 or 70 MPa at temperatures above −7.9°C, and the higher sintering pressure did not result in further densification. The density peak pressure was defined to describe the lowest pressure that was necessary to achieve the full density of 920 kg m^{-3} as ice (Russell-Head and others, 1984; White and McCallum, 2018). The density peak pressure corresponding to the temperature of −7.9 and −12.5/−17.3°C was 70 and

https://doi.org/10.1017/jog.2022.11 Published online by Cambridge University Press

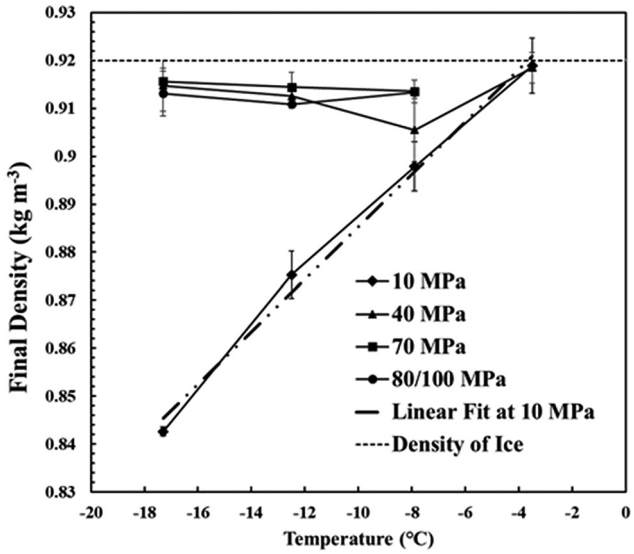

Fig. 3. Temperature dependence of final density sintered at various pressures.

40 MPa, respectively. Further experiments are required to confirm the density peak pressure at −3.5°C with sintering pressures below 10 MPa. The density of sintered snow increased with sintering pressure for the same duration of sintering time as was reported by Ebinuma and Maeno (1985) and Deimand and Klokov (2001). However, both of their experiments were not performed long enough for the sintered snow to reach ice density to make an accurate comparison with our results.

Effect of temperature on final density

The effect of sintering temperature on the final density of snow is shown in Figure 3. It was found that density decreased linearly with temperature at 10 MPa and fluctuated in a very narrow band at pressures above 70 MPa. The fitted line plot in Figure 3 illustrated the linear relationship between density ρ and temperature T as $\rho = 0.0055T + 0.9401$ with the R^2 value 99.2%. We concluded that the temperature has an impact on the transition of snow to ice in the pressure range below 10 MPa; however, more experiments need to be done at pressures between 10 and 40 MPa to figure out the exact pressure range within which temperature has an impact. It should be noted that the final density kinked at 40 MPa and −7.9°C, which requires a further microstructure study to understand the underlying mechanisms. The uncertainty in the offsets is, for example, the grain size of the snow. The final density at −3.5°C was close to ice density and relatively higher compared with the densities at other temperatures, indicating that the warmer temperature approaching the melting point favored snow sintering similar to the temperature effect on other materials (metal and ceramic). However, more experiments at temperatures from −3.5 to 0°C are required to conclude the effective temperature range for enhancing snow sintering.

Effect of the time on the relative density

Figure 4 shows the effect of time on the relative density at various temperatures and pressures with the three replicates. Since the initial density of each sample with the same setting varied slightly (Fig. 1), we opted not to calculate the average relative density during the densification process to illustrate randomness. Under the loading rate of 6.6 MPa min^{-1}, the pressure-acceleration period of 10, 40, 70, 80 and 100 MPa was finished at the time 1.5, 6.1, 10.6, 12.1 and 15.2 min, respectively, i.e. all the samples loaded the same at the first 1.5 min then reached to the pressure-holding period accordingly. In general, all curves in Figure 4 very closely resemble each other, exhibiting a short period of slow increase turning to a rapid increase in relative density with respect to loading time followed by slower increments prior to reaching maximum relative density. The time required to obtain the maximum relative density was stabilized within 20 min at various sintering parameters excluding at pressure 10 MPa. Although the maximum relative density correlates to the sintering temperature and warmer temperatures favor densification, at least 60 min was needed to sinter snow to ice at 10 MPa. The sintering kinetics occurred with relatively greater speed after sintering 1 min at pressures over 40 MPa with minor effect by temperatures on the time required to attain the maximum relative density. At −3.5°C and 40 MPa, the sintering kinetics were so rapid that 99.2% relative density was reached in 5 min. However, the ice under the pressure of 47 MPa melts at −3.5°C (Eqn (1)) resulting in a limitation to accelerate the sintering time by higher sintering pressure.

Relative significance of the sintering factors

The range analysis technique was used to determine the effects of sintering factors on final density and the optimum set of factors that would maximize final density. For the three sintering factors (pressure, temperature and sintering time), each factor was designed with four levels, as shown in Table 2. As the time required to reach 100 MPa at the loading rate of 6.6 MPa min^{-1} (3.5 kN min^{-1}) was ∼15 min, the sintering time level was from 15 to 60 min at 15 min intervals. An L_{16} (4^3) orthogonal array (Ross, 1996) was employed with the column assignment and the final density of sintered snow as shown in Table 3. Experiments 3 and 4 were not calculated because the experiment at pressures over 70 MPa for temperature −3.5°C was unable to be performed, limited by the ice pressure melting point. The range analysis of the sintered density is shown in Table 4, with K_{i1}, K_{i2}, K_{i3} and K_{i4}, corresponding to the sum of 1, 2, 3 and 4 level of i ($i = A, B, C$) factors, respectively. Also, k_{i1}, k_{i2} and k_{i3} correspond to the average values of 1, 2 and 3 level of i ($i = A, B, C$) factors, respectively, and R signifies the range corresponding to each factor, representing the degree of influence of various factors on the results.

The maximum and minimum range R indicates that pressure has the greatest impact on the final sintered density, followed by sintering time at temperatures between −3.5 and −17.3°C and sintering time longer than 15 min. The ice density could be effectively achieved through orthogonal experiment optimization with the appropriate parameter combination. The optimization for process parameters was conducted by the greatest density sintered at the level of factors. According to the optimization scheme on the final density, the best optimization scheme to sinter snow to ice is $A_2B_3C_1$ (−7.9°C, 70 MPa and 15 min). This does not conflict with the most rapid sintering kinetics found in this study at −3.5°C and 40 MPa within 5 min, as the sintering time in the range analysis was from 15 min (Table 2). From the optimization scheme of range analysis and the experimental results of sintering kinetics, the full density of sintered snow may be achieved either under higher pressure at a lower temperature with longer sintering time or under a lower pressure at a warmer temperature rapidly.

The evolution of relative density

The density evolution curves for snow at various temperatures and pressures are shown in Figure 5. The snow shows evident densification with increasing pressure reaching a maximum density, with its behavior overlapping during the pressure-acceleration

https://doi.org/10.1017/jog.2022.11 Published online by Cambridge University Press

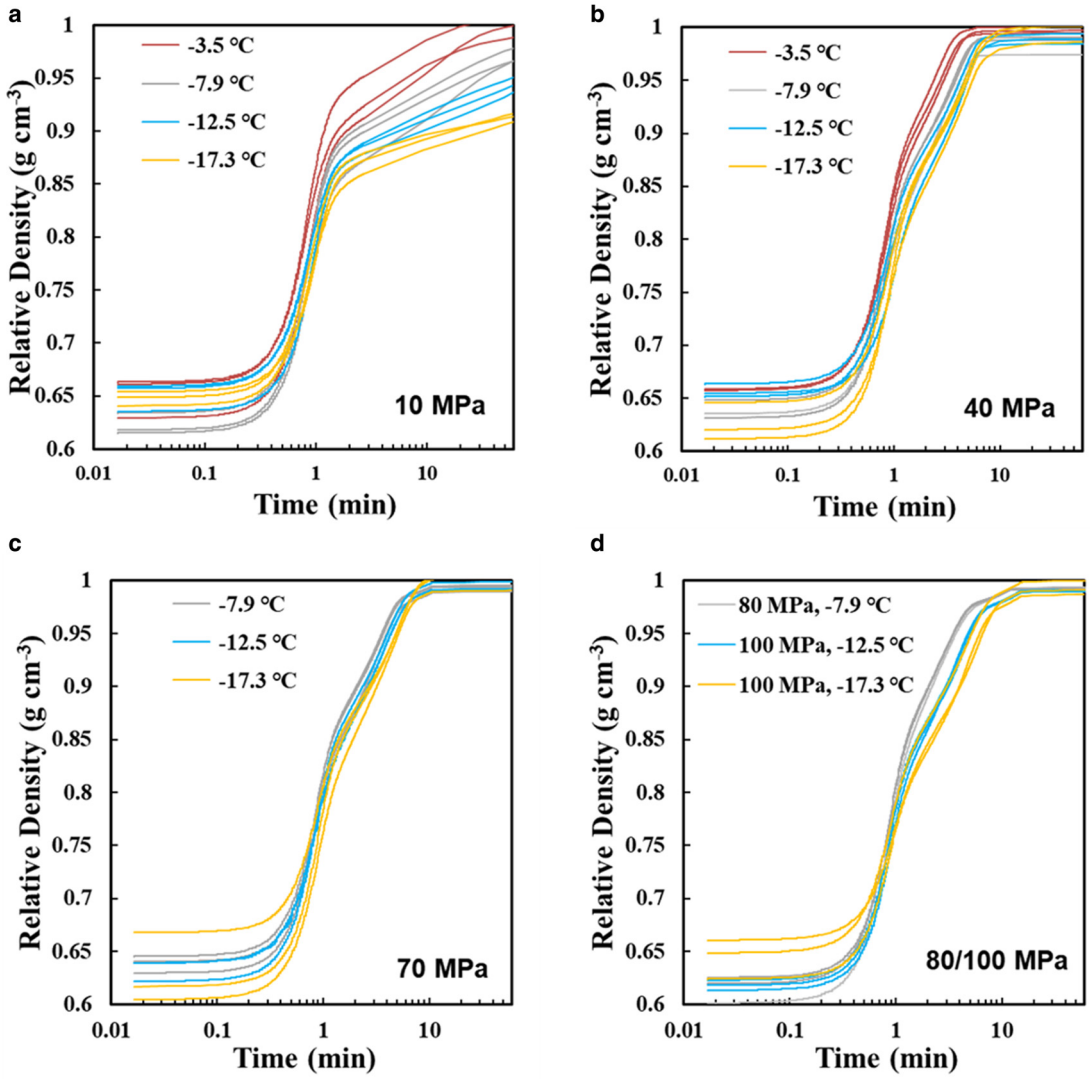

Fig. 4. Experimentally measured relative density versus time for ice under various pressures and temperature: (a) at 10 MPa; (b) at 40 MPa; (c) at 70 MPa; (d) at 80 MPa for −7.9°C, 100 MPa for −12.5 and −17.3°C. Note that the pressure melting point at 100 MPa is −7.41°C close to −7.9°C. The highest sintering experiment pressure for −7.9°C was chosen at 80 MPa.

Table 2. Factors and levels for the sintering experiments

Factor		Level 1	Level 2	Level 3	Level 4
A	Temperature (°C)	−3.5	−7.9	−12.5	−17.3
B	Pressure (MPa)	10	40	70	80/100
C	Sintering time (min)	15	30	45	60

Table 3. Orthogonal experiment scheme

Factor			Replication, density (g cm^{-3})			
A	*B*	*C*	*R*1	*R*2	*R*3	Average
1	1	1	0.885	0.876	0.907	0.889
1	2	2	0.894	0.915	0.917	0.909
1	3	3	–	–	–	–
1	4	4	–	–	–	–
2	1	2	0.873	0.888	0.878	0.880
2	2	3	0.896	0.909	0.911	0.905
2	3	4	0.910	0.915	0.916	0.914
2	4	1	0.913	0.912	0.912	0.912
3	1	3	0.868	0.861	0.853	0.861
3	2	4	0.910	0.906	0.914	0.91
3	3	1	0.912	0.911	0.919	0.914
3	4	2	0.912	0.910	0.910	0.911
4	1	4	0.836	0.843	0.840	0.840
4	2	1	0.901	0.917	0.913	0.910
4	3	2	0.911	0.922	0.924	0.919
4	4	3	0.908	0.912	0.919	0.913

period. There are two ways by which maximum density may be attained at the pressure holding period. For instance, the snow was able to sinter to a higher density during the pressure-holding period at 10 MPa from −3.5 to −17.3°C, and at 40 MPa from −7.9 to −17.3°C. However, the snow completed sintering and obtained maximum density as soon as the pressure reached 70, 80 or 100 MPa at temperatures of −7.9, −12.5 and −17.3°C, and 40 MPa at −3.5°C.

We can conclude from Figure 5 that the density evolution at pressures between 10 and 40 MPa to reach maximum final density depended largely on temperature during snow sintering. From Figure 2, the maximum final density under 10 and 40 MPa is attained at −3.5 and −3.5/−17.3°C, respectively. The sintering of snow at 40 MPa and −3.5°C may contain more liquid water compared with colder temperatures (>−3.5°C) due to the ice melting point was decreased to −2.958°C by pressure melting; this is in line with the theory that the compressibility of wet snow increases at a larger liquid content due to the higher

https://doi.org/10.1017/jog.2022.11 Published online by Cambridge University Press

Table 4. Range analysis of sintered density

Factors	*A*	*B*	*C*
K_{i1}	1.798	3.47	3.625
K_{i2}	3.611	3.634	3.619
K_{i3}	3.596	2.747	2.679
K_{i4}	3.582	2.736	2.664
k_{i1}	0.899	0.868	0.906
k_{i2}	0.903	0.909	0.905
k_{i3}	0.899	0.916	0.893
k_{i4}	0.896	0.912	0.888
R	0.007	0.048	0.018
Optimal levels	A_2	B_3	C_1
Primary and secondary order	$B > C > A$		
Optimal combination	$A_2B_3C_1$		

phase-equilibrium temperature of the stress-free surfaces enhanced by pressure melting at stressed surfaces (Colbeck, 1979). During the pressure-holding period, snow was sintered at 10 and 40 MPa to a higher density with a maximum density increase from 87 to 98% sintered at 10 MPa and −3.5°C, and from 97 to 100% at 40 MPa and −17.3°C, respectively. The underlying reason that during pressure-holding period warmer temperature favors snow to ice transition at a lower pressure (10 MPa) while a colder temperature benefits snow transition to ice at higher pressure (40 MPa) may be owing to two mechanisms: relatively more liquid content at 40 MPa and −3.5°C, and particle rearrangement as reported by Liu and DeLo (2001) during Ti-6Al-4V powder compaction. However, more experiments are required to emphasize the role of temperature on these phenomena. Schleef and Löwe (2013) found that the initial density of snow varied only by 0.01 g cm^{-3} causing a 12–16% densification rates change over the 2 d observation. Specific surface area decrease clearly contributes to the densification in the absence of an externally applied overburden stress, while it is affected neither by the initial density nor by densification during creep for any of the applied stresses between 0 and 318 Pa. It is likely that the variability between replicates caused by the initial density or the grain size/structure of the snow can cause the offsets on the evolution of relative density.

Uniaxial compressive behavior of sintered snow

The samples for unconfined uniaxial compression experiments were sintered at 70 MPa and −12.5°C for 20 min to reach the maximum density, achieving an average density of 0.914 kg m^{-3}. The samples had a cylindrical shape with a diameter of 26 mm and an average height of 66.9 ± 1 mm.

Figure 6 shows the stress–strain curves for sintered snow at strain rates from 5×10^{-4} to 10^{-1} s^{-1}. At lower strain rates, i.e. at strain rates lower than 5×10^{-3} s^{-1}, the stress linearly increases with the strain at first, and then the slope of the curve gradually decreases, becomes zero and then becomes negative; that is, the stress exhibits a rounded peak. All recovered samples deformed at strain rates lower than 5×10^{-3} s^{-1} either like a barrel where the central section was bulged or like a foot where the upper or lower part was bulged, showing ductile behavior (Fig. 7). At high strain rates, i.e. above 5×10^{-2} s^{-1}, the stress first increases linearly with the strain, reaching a sharp peak accompanied by a sudden stress drop to zero. All recovered samples deformed at strain rates over 5×10^{-2} s^{-1} broke along the axis of compression into one main part and many small pieces due to axial splitting (Fig. 7). At the strain rate 10^{-2} s^{-1}, the stress increases linearly at first and then reaches a maximum, but after the peak the stress decreases abruptly but does not drop suddenly to zero. The recovered samples did not break completely; that is, some cracks were observed on the side surface of the sample, and no cracks were observed in the center, showing combined ductile and brittle character (Fig. 7). The shape of the stress–strain curve corresponding to the macroscopic appearance of the deformed sample indicates a change of sintered snow from ductile behavior to brittle behavior as the strain rate increases. The transitional strain rate when the stress–strain curve shows the feature of both ductile and brittle dual-like behavior is at 10^{-2} s^{-1}, consistent with results of Arakawa and Maeno (1997) at −10°C.

Figure 8 shows the relationship between the compressive strength and the strain rate. The compressive strength increases with strain rate in the ductile region to a maximum at ductile-to-brittle transition and then drops in the brittle region. The strain rate-sensitive behavior of snow-sintered ice is consistent with previous reports from Yasui and others (2017) and Schulson and Duval (2009). In the ductile region, the compressive strength σ_f can be described by the power law $\sigma_f = (\dot{\varepsilon}/B)^{1/n}$, and increased by a power of $1/n$ with increasing strain rate. The values for the stress exponent n and the constant B, as derived from Figure 7 in this study and Yasui and others (2017), are presented in Table 5. The stress exponent, n, for snow-sintered ice was ~2 times larger than that of water-frozen ice, however, similar to 18% silica ice. The compressive strength of snow-sintered ice and water-frozen ice was estimated by power laws in Table 5 at 10^{-5} and 10^{-4} s^{-1} and at 5×10^{-4} and 5×10^{-3} s^{-1}, respectively. The R^2 of the power law fitting relationship of snow-sintered ice and water-frozen ice is 0.9997 and 0.9705, respectively. In making this comparison with the extrapolation, we found that the compressive strength of snow-sintered ice was ~1.2–2.2 times as large as that of water-frozen ice reported by Yasui and others (2017) with decreasing strain rate from 5×10^{-3} to 10^{-5} s^{-1}. The time required to fabricate a sample with a diameter of 30 mm and a height of 60 mm prepared by the water-frozen method at −10°C in Yasui and Arakawa (2008) was not specified. The freezing rate of ice grain and water mixture was ~2.8 μm s^{-1} by radial freezing method at −4.5°C reported by Cole (1979). At least 1.3 h are required to fabricate an ice sample with a diameter of 26 mm. However, with the high-pressure sintering method, as short as 5 min is enough to obtain the ice sample with the same diameter and similar or even higher compressive endurance.

Practical application perspectives

This research provides valuable data, which go beyond former studies and connects snow density evolution to high-pressure applications. Moreover, this study offers insight into strategies to produce fast compacted snow that can be used for construction in polar regions.

(1) The snow density can be controlled scientifically regarding the snow strength for the design of polar infrastructure according to the sintering effect of snow under various pressures as a function of time and temperature. The construction time in the harsh environment can be minimized reasonably by choosing the optimal equipment with appropriate compaction load depending on in situ natural atmospheric temperatures, and is affected by the snow density varied from site to site in the polar regions.
(2) Considering the increased rates of ice fabrication, low limitations on temperature, and reliable sintered snow strength, high-pressure sintering is beneficial for easy, broad and efficient utilization of snow as a promising material for construction in polar regions.

Conclusions

The snow sintering experiments were performed under a high strain rate of 10^{-4} s^{-1} and a wide pressure range up to 100 MPa

https://doi.org/10.1017/jog.2022.11 Published online by Cambridge University Press

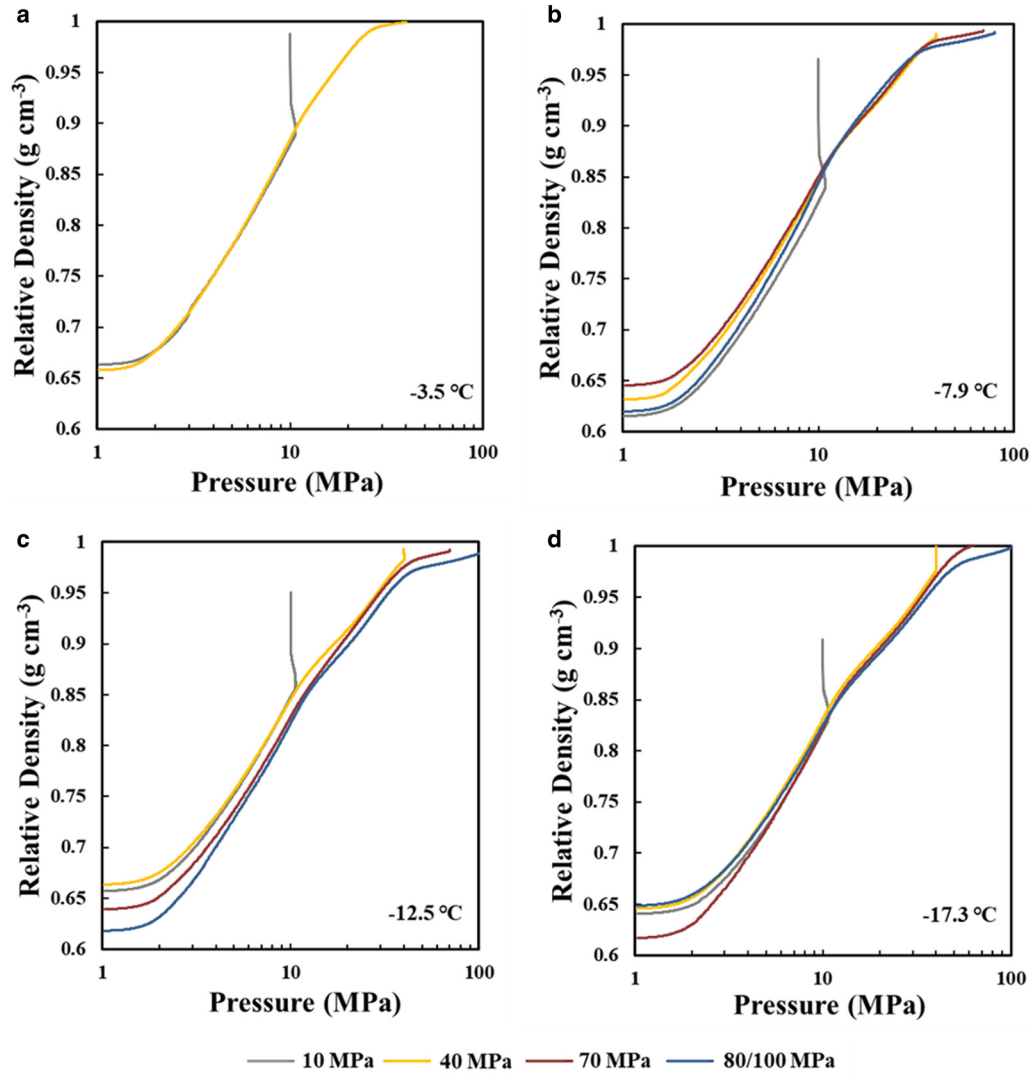

Fig. 5. Relative density–pressure relationships at different temperatures using one of the three replications as a representation: (a) at −3.5°C; (b) at −7.9°C; (c) at −12.5°C; (d) at −17.3°C.

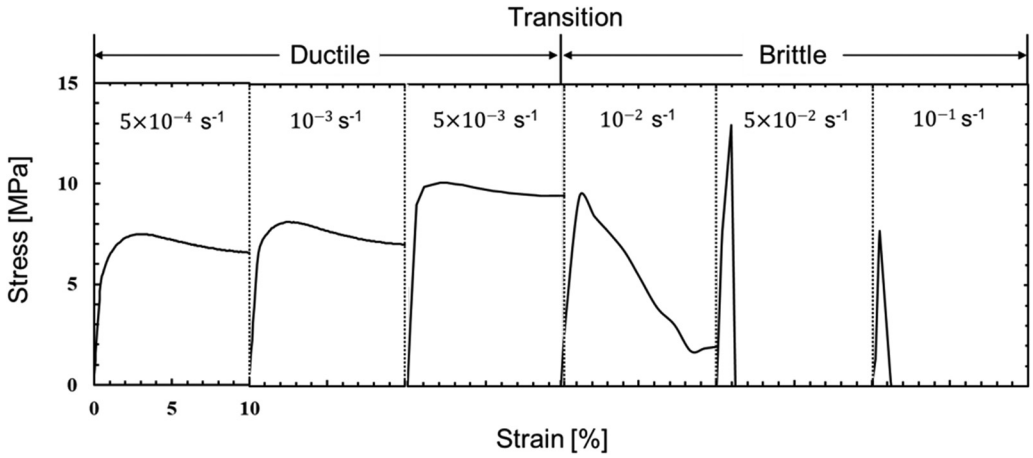

Fig. 6. Stress–strain curves of sintered snow. The curves on each figure are lined up in order of strain rate. Three types of deformation (ductile, ductile-to-brittle transition and brittle) show on the top of the figure.

at temperatures between −3.5 and −17.3°C. The density transition from snow to ice may be achieved under higher pressure in a wide temperature range within the limits of the ice pressure melting point and the performance of the available equipment for snow sintering. Range analysis of the orthogonal experiment showed that pressure affected the final density significantly in comparison with sintering temperature and time. The final density of sintered snow showed no significant difference in terms of variations in sintering temperature and pressure when a pressure above 40 MPa was used to press snow. This is important as the use of

https://doi.org/10.1017/jog.2022.11 Published online by Cambridge University Press

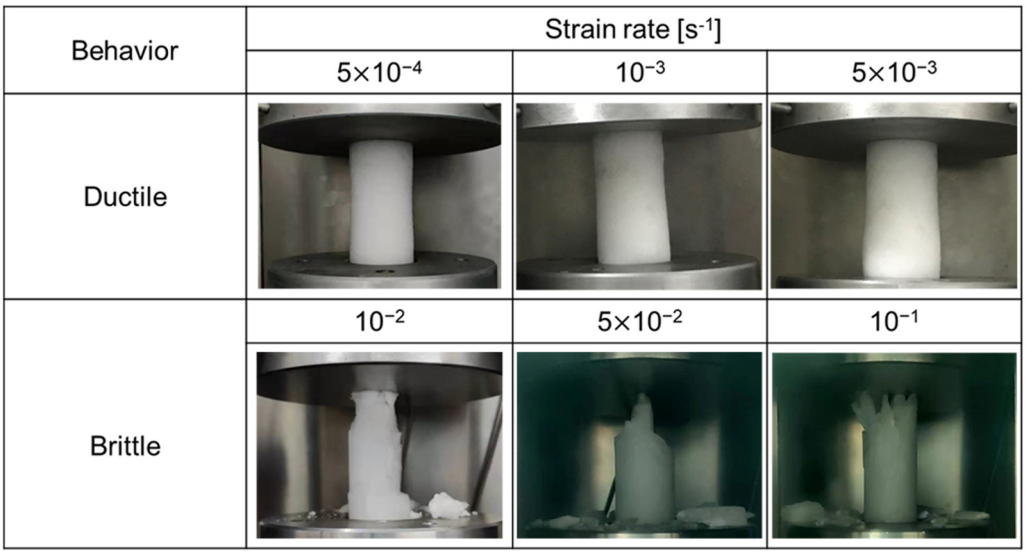

Fig. 7. Images of compressed samples showing ductile and brittle macroscopic appearance of the deformed sample at strain rate ranged from 5×10^{-4} to 10^{-1} s^{-1}.

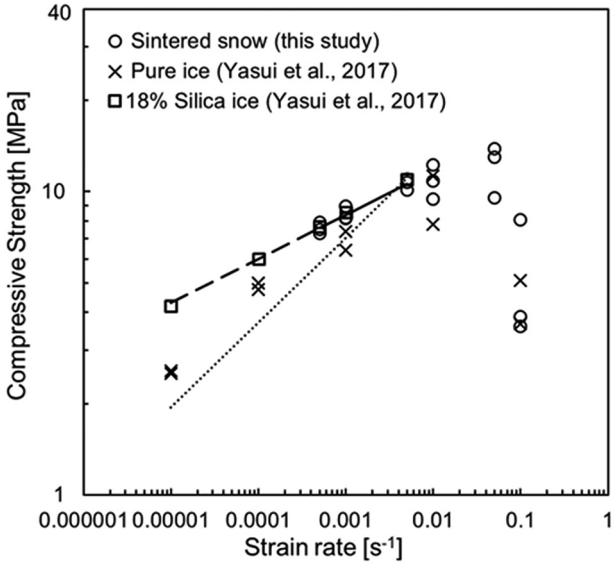

Fig. 8. Compressive strength of sintered snow, pure ice and silica ice versus strain rate. The 'cross' and 'square' symbols showing 'pure ice' and '18% silica ice' present the results of Yasui and others (2017). The lines are fitted by $\sigma_f = (\dot{\varepsilon}/B)^{1/n}$ according to the least-squares method. The solid line is fitted by using our results in a ductile regime (strain rate smaller than 5×10^{-3} s^{-1}) and extrapolated to 10^{-5} with a dashed line. The dotted line is fitted using the results of Yasui and others (2017).

Table 5. Constants B and n in the power law describing ductile behavior (Yasui and others, 2017)

Ice type	n	B (s^{-1} MPa^{-n})
Snow-sintered ice	6.87	4.50×10^{-10}
Water-frozen ice	3.57	9.33×10^{-7}
18% Silica ice	6.48	9.14×10^{-10}

low pressures may positively impact the lifetime of the dies, generating economic benefits (e.g. die abrasion frequency, equipment load capacity and so on) from a practical point of view.

Uniaxial compression experiments were performed under constant strain rates from 5×10^{-4} to 10^{-1} s^{-1} at the temperature of −10°C. The shape of the stress–strain curve corresponding to the macroscopic appearance of the deformed sample indicates a change of sintered snow from ductile behavior to brittle behavior as the strain rate increases. The transitional strain rate showing the feature of both ductile and brittle dual-like behavior is at 10^{-2} s^{-1}. The compressive strength increases with strain rate in the ductile region to a maximum at ductile-to-brittle transition and then drops in the brittle region. The compressive strength of snow-sintered ice was ~1.2–2.2 times as large as that of water-frozen ice reported by previous work with decreasing strain rate from 5×10^{-3} to 10^{-5} s^{-1}. The increased rates of ice fabrication, low limitations on temperature and reliable sintered snow strength indicate that snow-ice engineering, such as airport construction in Greenland and Antarctica and the foundation for Arctic ice-shelf development, can be improved by high-pressure sintering of snow to overcome the harsh environment.

Acknowledgements. This paper presents the results of the research conducted with support from the National Natural Science Foundation of China (grant No. 41806220, 41941005); State Key Laboratory of Cryospheric Science, Northwest Institute of Eco-Environment and Resources, Chinese Academy Sciences (grant No. SKLCS-OP-2020-01); the Ministry of Science and Technology of the People's Republic of China (grant No. 2016YFC1400300); and the Program for Jilin University Science and Technology Innovative Research Team (grant No. 2017TD-24).

Conflict of interest. The authors declare that they have no known competing financial interests or personal relationships that could have appeared to influence the work reported in this paper. The authors are unaware of any conflicts of interest regarding the data and findings presented in this manuscript.

References

Abele G (1990) *Snow Roads and Runways*, Vol. **90**. No. 3. Hanover: US Army Cold Regions Research and Engineering Laboratory.

Abele G and Frankenstein GE (1967) *Snow and Ice Properties as Related to Roads and Runways in Antarctica*, Vol. **176**. Hanover: US Army Cold Regions Research and Engineering Laboratory.

Abele G, Ramseier RO and Albert FW (1968) *Design Criteria for Snow Runways*. Hanover: US Army Cold Regions Research and Engineering Laboratory.

Albert FW (1963) *Snow Stabilization for Roads and Runways* (Research Report 83). Hanover: Cold Regions Research and Engineering Laboratory, US Army Cold Regions Research and Engineering Laboratory.

Arakawa M and Maeno N (1997) Mechanical strength of polycrystalline ice under uniaxial compression. *Cold Regions Science and Technology* **26**, 215–229. doi: 10.1016/S0165-232X(97)00018-9

Arzt E, Ashby MF and Easterling KE (1983) Practical applications of hotisostatic pressing diagrams: four case studies. *Metallurgical and Materials Transactions A* **14**(1), 211–221. doi: 10.1007/BF02651618

Colbeck SC (1979) Sintering and compaction of snow containing liquid water. *Philosophical Magazine A-Physics of Condensed Matter Structure Defects and Mechanical Properties* **39**, 13–32. doi: 10.1080/01418617908239272

Cole DM (1979) Preparation of polycrystalline ice specimens for laboratory experiments. *Cold Regions Science and Technology* **1**(2), 153–159. doi: 10.1016/0165-232X(79)90007-7

Diemand D and Klokov V (2001) A method for producing fine-grained ice from snow by compaction, CRREL TR-01-12, US Army Cold Regions Research and Engineering Laboratory, Hanover.

Ebinuma T and Maeno N (1985) Experimental studies on densification and pressure-sintering of Ice. *Annals of Glaciology* **6**, 83–86. doi: 10.3189/1985aog6-1-83-86

Ebinuma T and Maeno N (1987) Particle rearrangement and dislocation creep in a snow-densification process. *Le Journal de Physique Colloques* **48**(C1), 263–269.

German RM (2014) Future prospects for sintering. In *Sintering: From Empirical Observations to Scientific Principles*, German RM (ed.), pp. 513–526. Amsterdam: Elsevier. doi: 10.1016/b978-0-12-401682-8.00016-1

Kingery WD (1960) Applied glaciology – the utilization of ice and snow in Arctic operations. *Journal of Glaciology* **3**(27), 577–588. doi: 10.3189/s0022143000023704

Liu J and DeLo DP (2001) Particle rearrangement during powder compaction. *Metallurgical and Materials Transactions A Physical Metallurgy and Materials Science* **32**, 3117–3124. doi: 10.1007/s11661-001-0186-7

Maeno N and Ebinuma T (1983) Pressure sintering of ice and its implication to the densification of snow at polar glaciers and ice sheets. *Journal of Physical Chemistry* **87**, 4103–4110. doi: 10.1021/j100244a023

Meyer CR, Keegan KM, Baker I and Hawley RL (2020) A model for French-press experiments of dry snow compaction. *Cryosphere* **14**(5), 1449–1458. doi: 10.5194/tc-14-1449-2020

Paterson KCWSB (2010) *The Physics of Glaciers*. Cambridge: Cambridge University Press.

Ramseier RO (1966) *Temperature Dependence and Mechanism of Sintering* (Res Rep 189). Hanover: US Army Cold Regions Research and Engineering Laboratory.

Ramseier RO (1967) *Role of Sintering in Snow Construction* (Research Report 214). Hanover: US Army Cold Regions Research and Engineering Laboratory.

Ross PJ (1996) *Taguchi Techniques for Quality Engineering: Loss Function, Orthogonal Experiments, Parameter and Tolerance Design*. New York: McGraw-Hill.

Russell-Head DS, Budd WF and Moore PJ (1984) Compacted snow as a pavement material for runway construction. *Cold Regions Science and Technology*. doi: 10.1016/0165-232X(84)90070-3

Salamatin AN and 5 others (2009) Snow-firn densification in polar ice sheets. *Physics of Ice Core Records* **68**, 195–222.

Schleef S and Löwe H (2013) X-ray microtomography analysis of isothermal densification of new snow under external mechanical stress. *Journal of Glaciology* **59**(214), 233–243. doi: 10.3189/2013JoG12J076

Schulson EM and Duval P (2009) *Creep and Fracture of Ice*. Cambridge: Cambridge University Press, p. 401.

Tobiasson W and Donald LR (1966) *A Straight-Wall Cut-and-Cover Snow Trench*, Vol. **151**. Hanover: US Army Cold Regions Research and Engineering Laboratory.

Wang X and Baker I (2013) Observation of the microstructural evolution of snow under uniaxial compression using X-ray computed microtomography. *Journal of Geophysical Research. Atmospheres: JGR* **118**, 12371–12382. doi: 10.1002/2013JD020352

White G and McCallum A (2018) Review of ice and snow runway pavements. *International Journal of Pavement Research Technology* **11**, 311–320. doi: 10.1016/j.ijprt.2017.11.002

Yasui M and Arakawa M (2008) Experimental study on the rate dependent strength of ice-silica mixture with silica volume fractions up to 0.63. *Geophysical Research Letters* **35**, L12206. doi: 10.1029/2008GL033787

Yasui M, Schulson EM and Renshaw CE (2017) Experimental studies on mechanical properties and ductile-to-brittle transition of ice-silica mixtures: Young's modulus, compressive strength, and fracture toughness. *Journal of Geophysical Research: Solid Earth* **122**(8), 6014–6030. doi: 10.1002/2017JB014029

https://doi.org/10.1017/jog.2022.11 Published online by Cambridge University Press